Transcriptional mapping of the macaque retina and RPE-choroid reveals conserved inter-tissue transcription drivers and signaling pathways

Ameera Mungale[1#], David M. McGaughey[2#], Congxiao Zhang[3], Sairah Yousaf[1], James Liu[1], Brian P. Brooks[4], Arvydas Maminishkis[3], Temesgen D. Fufa[1], Robert B. Hufnagel[1*]

[1]Medical Genetics and Ophthalmic Genomics Unit, Ophthalmic Genetics and Visual Function Branch, National Eye Institute, National Institutes of Health
[2]Bioinformatics Group, Ophthalmic Genetics and Visual Function Branch, National Eye Institute, National Institutes of Health
[3]Section on Epithelial and Retinal Physiology and Disease, Ophthalmic Genetics and Visual Function Branch, National Eye Institute, National Institutes of Health
[4]Pediatric, Developmental & Genetic Ophthalmology Section, Ophthalmic Genetics and Visual Function Branch, National Eye Institute, National Institutes of Health

[#]Equal contributors

*Correspondence: Robert B. Hufnagel (robert.hufnagel@nih.gov): 10 Center Drive, rm 10N109, Bethesda, MD 10N109.

Running title: Conserved primate macular transcriptome

46 **Abstract**

47 Purpose: The macula and fovea comprise a highly sensitive visual detection tissue that is
48 susceptible to common disease processes like age-related macular degeneration (AMD). Our
49 understanding of the molecular determinants of high acuity vision remains unclear, as few model
50 organisms possess a human-like fovea. We explore transcription factor networks and receptor-
51 ligand interactions to elucidate tissue interactions in the macula and peripheral retina and
52 concomitant changes in the underlying retinal pigment epithelium (RPE)/choroid.

54 Methods: Poly-A selected, 100 bp paired-end RNA-sequencing (RNA-seq) was performed
55 across the macular/foveal, perimacular, and temporal peripheral regions of the neural retina and
56 RPE/choroid tissues of four adult Rhesus macaque eyes to characterize region- and tissue-
57 specific gene expression. RNA-seq reads were mapped to both the macaque and human genomes
58 for maximum alignment and analyzed for differential expression and Gene Ontology (GO)
59 enrichment.

61 Results: Comparison of the neural retina and RPE/choroid tissues indicated distinct, contiguously
62 changing gene expression profiles from fovea through perimacula to periphery. Top GO
63 enrichment of differentially expressed genes in the RPE/choroid included cell junction
64 organization and epithelial cell development. Expression of transcriptional regulators and various
65 disease-associated genes show distinct location-specific preference and retina-RPE/choroid
66 tissue-tissue interactions.

68 Conclusions: Regional gene expression changes in the macaque retina and RPE/choroid is
69 greater than that found in previously published transcriptome analysis of the human retina and
70 RPE/choroid. Further, conservation of human macula-specific transcription factor profiles and
71 gene expression in macaque tissues suggest a conservation of programs required for retina and
72 RPE/choroid function and disease susceptibility.

73   **Introduction**
74   The retina is a thin tissue of the posterior eye (range: 166.9 ± 20.9 μm - 271.4 ± 19.6 μm[1]
75   essential for processing light and transmitting information to the brain through the optic nerve. It
76   is composed of multiple layers, which contain seven cell classes including rod and cone
77   photoreceptors, in apposition with the retinal pigment epithelium (RPE), which is underlaid by
78   the choroid. The choroid is a vascular structure that supports the outer retina, the RPE is
79   necessary for maintaining healthy photoreceptors, and rods mediate dark-adapted vision while
80   cones are responsible for color vision[2, 3]. The relative composition of cell types varies across
81   the retina, and provides visual function specializations, such as high acuity color vision at the
82   fovea, which is cone photoreceptor rich and rod depleted. Furthermore, the neural retinal layers
83   change in thickness and morphology, including the inner and outer nuclear layers of the
84   photoreceptors, whereas the choroidal layer has increased thickness at the macula but the
85   morphology of the entire layer remains relatively unchanged[4, 5]. Many genes have varied
86   expression in different cell types and tissue layers, with 819 genes implicated in heritable retinal
87   degenerations as of 2022 (RetNet, https://sph.uth.edu/RetNet/)[6, 7]. While retinal degeneration
88   may initiate in a single tissue layer, eventually the disease progresses across all tissue layers [8].
89   Importantly, retinal manifestations in many diseases are region specific. For example, Stargardt
90   disease and Best disease primarily affect the macula and cause loss of central vision first,
91   whereas retinitis pigmentosa initiates in the rod-rich periphery[9-12]. We hypothesize that this
92   location-specific disease susceptibility of the retina is due to cellular specialization and region-
93   dependent molecular interactions, which we can assess by regional layer-specific gene
94   expression profiling of healthy retinae.
95
96   Previous investigations of the transcriptomic landscape of the human retina support a significant
97   differential gene expression between the retina and the RPE/choroid/sclera tissue layers as well
98   as across macular and peripheral regions, as described by Li et al., 2014[13]. Comparison of
99   gene expression between the nasal and temporal peripheries of retina and RPE/choroid/sclera
100   tissues indicated little to no variability, yet macular and peripheral profiles remained distinct in
101   each tissue[13]. Gene expression across the retina has shown to be consistent with the spatial
102   distribution of photoreceptors and ganglion cells, and RPE-specific genes appear to be enriched
103   in the periphery over the macula as outlined by Whitmore et al., 2014[14]. Further
104   characterization of gene expression between foveal and peripheral retina has been conducted
105   using single-cell RNA sequencing in both primate (*Macaca fascicularis*) by Peng et al., 2019[15]
106   and human retina by Voight et al., 2019[16]. These studies showed variability in both cell type
107   distribution and gene expression between foveal and peripheral retina[15, 16]. While it has been
108   well established that regional differences exist across tissue layers in the primate retina, the
109   molecular drivers of these differences remain unclear.
110
111   Here we generate an RNA-seq dataset from adult Rhesus macaque (*Macaca mulatta*) eyes that
112   reflect the changing photoreceptor composition of the contiguous macular/foveal, perimacular,
113   and peripheral regions to determine tissue- and location-dependent differential gene expression
114   of the neural retina and RPE/choroid. The use of matched retina and RPE/choroid tissue biopsies
115   in this analysis with an additional perimacular sample provides a contiguous assessment of gene
116   expression across location as opposed to a binary macular vs periphery comparison and allows
117   for a more comprehensive look at patterns of gene expression and their related pathways and

118 ontologies. We additionally explore conservation of these shared and distinct pathways through a
119 meta-analysis comparing our macaque datasets to previously published human data. Finally, we
120 examine gene regulation via transcription factors and tissue-tissue interactions using
121 ligand/receptor analysis to understand differences in the macular and peripheral retina and the
122 affiliated changes in the RPE/choroid.
123
124 **Methods**
125
126 Animal Care
127 All experimental protocols were approved by the National Eye Institute Animal Care and Use
128 Committee. Procedures were performed in accordance with the United States Public Health
129 Service policy on the humane care and use of laboratory animals.
130
131 Tissue Acquisition
132 Postmortem eyes were enucleated from two adult Rhesus monkeys (*Macaca mulatta)*, aged 13
133 and 18 years. Two-millimeter punch biopsies were removed from macular/foveal, perimacular,
134 temporal, and nasal regions of the retina. Following the biopsy, the tissues were separated into
135 layers of neural retina and RPE/choroid using microdissection techniques. Biopsies were
136 optimized for smallest diameter in other macaque samples in order to obtain the minimal number
137 of cells required for RNA-sequencing. Optimization was performed by measuring total RNA
138 yield in different sized biopsy samples as below and requiring a minimum of 200 ng as input for
139 RNA-seq.
140
141 RNA Extraction

142 Total RNA was isolated from fresh tissues using the PicoPure™ RNA Isolation Kit (Applied
143 Biosystems, Waltham, Massachusetts, USA) following mortar and pestle tissue homogenization.
144 Extracted RNA samples were checked for quality using the 2100 Bioanalyzer (Agilent
145 Technologies, Santa Clara, CA, USA) and only samples with RIN value > 6.5 were used (Range
146 1 – 10).

147
148 RNA sequencing
149 Extracted RNA was prepared into 100 bp libraries for paired-end, poly-A-selected RNA
150 sequencing on the Illumina HiSeq4000 at the NIH Intramural Sequencing Center.
151
152 Bioinformatic Analysis
153 Briefly, reads were quantified against the macaque genome Mmul_8.0.1 using Salmon pseudo-
154 alignment transcript quantification tool (version 0.13.0; Patro et al., 2017)[17], imported into R
155 with tximport[18] and analyzed for differential expression using DESeq2, using the Rhesus
156 macaque sample as a covariate [19]. Transcript reads were additionally aligned to the human
157 genome (GRCH38, gencode version 30 [20], to supplement any unquantified genes. To select the
158 gene name for each macaque transcript, we used the HGNC Comparison of Orthology
159 Predictions[21] data, aggregated by the hcop R package (https://github.com/stephenturner/hcop).
160 We counted the number of sources supporting each gene ID to transcript and selected the gene
161 ID with the most support, as detailed in https://github.com/davemcg/macaque_macula_RNA-
162 seq/blob/master/analysis/01_QC_prelim_analysis.Rmd.
163

164 Genes were considered to be differentially expressed based on IHW[22] corrected p value <
165 0.05. Gene lists were then assigned gene ontologies using the clusterProfiler "enrichGO"
166 function[23].
167
168 For the heatmap visualizations, we used length-scaled transcripts per million (TPM)
169 quantification from tximport scaled by library size with the edgeR[24] "calcNormFactors"
170 function. The heatmaps were made with the R package ComplexHeatmap[25].
171
172 Human single cell transcriptome data from the scEiaD resource at plae.nei.nih.gov was searched
173 for machine predicted RPE cells from fovea or peripheral punches. We found 217 cells, 159
174 from the fovea and 58 from the periphery, across four studies[26-30]. The Seurat object was
175 downloaded on 2022-01-14 from plae.nei.nih.gov and subsetted to these 217 cells. The Seurat
176 object was converted to a SingleCellExperiment object to run wilcox and t tests with the scran
177 "findMarkers" test and used the study as a covariate. Genes were kept which had both a wilcox
178 AUC (area under curve) greater than 0.7 (1 is best), an abs(log2)fold change greater than 0.7, and
179 a FDR corrected p value < 0.01. For the overlap testing we kept genes that had a padj < 0.01 in
180 each comparison (single cell human RPE, bulk human RPE-choroid, or bulk macaque RPE-
181 choroid) and the direction of the fold change between fovea and peripheral was the same. The
182 venn diagram was created with the R package eulerr (https://cran.r-
183 project.org/web/packages/eulerr/citation.html).
184
185 For the exact commands used in the analysis of this data, we make our Snakemake[31]
186 reproducible workflow available at https://github.com/davemcg/macaque_macula_RNA-seq.
187
188 **Results**
189
190 We performed RNA-seq on 2 mm retina and RPE/choroid tissues of 4 adult Rhesus macaque
191 eyes in each of the central macular (foveal), perimacular, and peripheral regions (Fig. S1). Tissue
192 dissections and RNA extractions were optimized for minimal input samples (<1 μg) to maximize
193 spatial resolution. Principle component analysis (PCA) visualization indicates that samples group
194 primarily by tissue. Foveal and peripheral samples generally cluster furthest from each other, and
195 perimacular samples cluster in between (Fig. S2). We then assessed overall gene expression by
196 tissue layer and location as well as differential gene expression between foveal samples and other
197 peripheral samples (Table 1).
198
199 Analysis of the foveal versus peripheral regions in the retina and RPE/choroid depicted distinct
200 sets of differentially expressed genes in each tissue layer, with 9644 and 7925 differentially
201 expressed genes in the retina and RPE/choroid, respectively (Padj < 0.05) (Table 1). Many of the
202 significantly differentially expressed genes are known to have tissue-specific roles in
203 development and disease (Fig. 1A, 1B). Retinal diseases also manifest uniquely at particular
204 regions of the RPE or retina. For example, Age-Related Macular Degeneration (AMD) is thought
205 to begin in the macular RPE[32], Late Onset Retinal Degeneration manifests in the peripheral
206 RPE[33], Retinitis Pigmentosa causes photoreceptor loss in the peripheral retina[10], and finally,
207 Cone-Rod Dystrophies primarily affect photoreceptors in the central retina[34].
208

209   In order to confirm that the differentially expressed genes across locations further reflect cellular
210   composition of different tissues, we used expression patterns of published rod-enriched genes as
211   identified in Holt et al., 2015[6] and Mustafi et al., 2016[35]. We observed correlated gene
212   expression between eyes and animals, as well as a progressive increase in rod-enriched gene
213   expression from the fovea to the perimacula and then to the periphery, reflecting changes in
214   neural retina composition (Fig. S3A). In this list of rod enriched genes, we find that our
215   peripheral retina samples are 2.8 fold enriched in rod signal relative to the fovea (t test $p < 3.5$ e-
216   12). The perimacular region was enriched in rod signal by 1.7 fold over the fovea ($p < 1.1$ e-09).
217   The enrichment of cone gene expression between the fovea and peripheral retina samples was
218   1.6 fold ($p < 0.02$) (Fig. S3B, Table S1). Among the RPE samples the enrichment of rod and
219   cone markers was less substantial and not significant (Figure S3C).
220

221   Next, we performed an unfiltered analysis of the differentially expressed, contiguously changing
222   genes from fovea to perimacula to periphery in the RPE/choroid. This analysis highlights
223   stepwise changes due to changing photoreceptor composition in the cone-predominant macula,
224   rod-predominant periphery, and admixed perimacula, and how these morphological changes in
225   the neural retina may affect changing gene expression in the RPE/choroid. Differential
226   expression analysis revealed distinct blocks of genes with low expression in the fovea that
227   increase moving outward through the perimacula to the periphery, and other genes that are
228   highly expressed in the fovea but progressively decrease moving outwards (Fig. 1C). We observe
229   enrichment for gene ontologies including cell junction organization and epithelial cell
230   development, as well as urogenital and renal system development (Fig. 1D).
231

232   Next, we sought to understand the transcriptional regulators driving the spatial and inter-tissue
233   differences in gene expression. Using a list of all known transcription factors in humans, we
234   identified a subset which is differentially expressed by location in each of the retina (Fig. S4B)
235   and RPE/choroid datasets (Fig. 1E). After conducting a literature review, we further identified
236   transcription factors with known associations in the respective tissues. In the retina and RPE,
237   distinct sets of fovea-enriched and periphery-enriched transcription were elucidated. Our data
238   shows three transcription factors, *NFRF1*, *IRX2*, and *ZFHX4*, to be differentially expressed in
239   both neural retina and RPE/choroid and show a similar pattern in independent human data
240   curated from eyeIntegration[36] (Fig. S5). Interestingly, *ZFHX4* appears to be enriched in the
241   macular neural retina and the peripheral RPE/choroid, whereas *NFRF1* and *IRX2* expression is
242   present in both tissues.
243

244   We then analyzed tissue-tissue interactions using ligand and receptor characterizations from the
245   CellPhoneDB database[37]. After converting protein names from the database to gene names via
246   the Uniprot conversion tool and merging the data with our location-based differential expression,
247   we generated lists of distinct up- and down-regulated interactions in which both interacting
248   partners in each tissue were either up- or downregulated in the fovea over the periphery (Table
249   2). Pathway analysis on these gene lists shows enrichment in the upregulated interactors for cell
250   adhesion pathways (Fig. 2A, C) and that downregulated interactors were highly enriched for Wnt
251   signaling in kidney disease and the ErbB signaling pathway, both of which are heavily involved
252   in tissue development, including ocular development (Fig. 2B, D, Fig. S7C-D).
253

254 To determine the conservation of location-specific differential expression of transcriptional
255 regulators across fovea to periphery, we performed a meta-analysis comparing our macaque data
256 to previously published human datasets[13, 14]. We see generally conserved patterns of
257 expression from fovea to periphery in neural retina and to a lesser extent, RPE/choroid (Fig. 3A-
258 B). We performed the same analysis on unfiltered gene lists from the human and macaque and
259 found approximately 700 genes that follow similar differential expression patterns from fovea to
260 periphery in both species. (Fig. 3A, Table 1S). GO terms for this list of conserved genes involve
261 neuronal connectivity and cellular morphogenesis (Fig. 3C), similar to the GO terms for the
262 macaque retina data seen previously in this study. In one case, we see a distinct block of macula-
263 specific transcription factors in the Rhesus monkey neural retina including *HR*, *MYC*, *EBF3*, *AR*,
264 *EBF2*, *EBF1*, *TWIST1*, *IRX2*, *POU4F2*, *IRX1*, and *SHOX2* that seem to also correlate to macula-
265 specific transcription factors in the human data (Fig. S6B). Overall, this supports a conservation
266 of gene expression and function across monkey and human species.
267
268 To test whether there was any correspondence between our macaque tests and an independent
269 single cell RPE cells taken from either the fovea or periphery, we extracted 219 cells from the
270 scEiaD resource at plae.nei.nih.gov. We found ten genes that overlap between our macaque
271 resource and the scEiaD resource, including *VIM*, *S100B*, and *PMEL*. Of these overlapping
272 genes, *CXCL4*, *SULF4*, and *WFDC1* are shown to be enriched in the macula (Figure 4).
273
274 **Discussion**
275
276 Using the Rhesus macaque as a model to study the transcriptome landscape of higher primate
277 retina, we conducted RNA-sequencing across neural retina and RPE/choroid tissue layers. The
278 small RNA punch size and bulk processing of the tissues allowed for high resolution and
279 sensitivity of transcript quantification due to the decreased likelihood of variability from
280 extended amplification, gene dropouts, and biological noise. Furthermore, it allows for the ability
281 to profile rare and low-expressed transcripts as compared to single-cell RNAseq such as the 10x
282 Genomics Chromium platform, in which only the top 20-30% of expressed genes are captured,
283 or Drop-seq, which requires a more manual approach. Unlike previous studies, our approach
284 included the perimacular retina to define contiguously changing gene expression across the
285 retinal landscape, thereby reflecting the stepwise differences in the ratio of cone and rod
286 composition. By doing this, we isolated the critical pathways regulating changes in retinal
287 connectivity and RPE/choroid function necessary to support different photoreceptor mosaics.
288
289 The macaque gene expression changes observed in our data are orthogonally confirmed in
290 human datasets. Furthermore, our findings also indicate conservation of contiguously changing
291 gene expression patterns from the central to peripheral retina between Rhesus monkeys and
292 humans, establishing a more available model system for future human transcriptomic studies.
293 Rhesus monkeys offer an accessible model in which conditions of tissue acquisition can be
294 further controlled, including age, optimization of biopsy and RNA extraction, and reduced time
295 from enucleation to tissue dissection and RNA extraction.
296
297 PCA of gene expression data by tissue type predicts the distinct nature of the neural retina and
298 RPE/choroid tissues, and further clustering by location confirms there are transcriptomic
299 differences between regions of the retina. The grouping of transcriptomes by animal highlights

300   the genetic variability observed between individuals. The lower number of differentially
301   expressed genes in fovea vs perimacular comparisons versus fovea vs periphery indicates a
302   continuum of gene expression. The highly variable patterns of gene expression across the neural
303   retina corresponds to the changing composition of cell types based on location.
304
305   In contrast, the presence of distinct changing RPE/choroid gene expression suggests variability
306   in the cell processes occurring across the retina in the RPE and choroid. Due to the relatively
307   unchanged morphology of these tissues across the retina save for increased RPE diameter and
308   choroidal thickness in the macula, the contiguous changes in gene expression observed may be a
309   factor in driving changes in cell processes across the entire retina. GO terms enriched for the
310   contiguously changing genes in the retina involved neuron projection and axon development as
311   well as regulation of cell morphogenesis, supporting known findings that there are differences in
312   circuitry and cone packing across the neural retina[10]. Furthermore, the changing gene
313   expression across the RPE/choroid is enriched for GO terms such as cell junction organization
314   and epithelial cell development, supporting reported findings that RPE diameter is smaller in the
315   fovea/macula as compared to the periphery[38]. It is known that RPE cells form tight junctions,
316   creating the outer blood-retinal barrier. These tight junctions serve as regulators of cell
317   proliferation, polarity, and transport, as well as transducers of signals responsible for regulating
318   cell size and shape[39]. Therefore, genes involved in cell junction organization and epithelial cell
319   development may play a role in varied cell sizes across the RPE. GO terms involving urogenital
320   and renal system development are also enriched in the RPE/choroid gene list, and interestingly,
321   there are several heritable genetic conditions that affect both the eye and kidney, and there is also
322   a link between chorioretinal thinning and chronic kidney disease, thought to be due to
323   inflammation and endothelial dysfunction[40, 41]. In addition to observing greater levels of gene
324   expression variability across location in the RPE-choroid than expected, several disease-relevant
325   genes known to play roles in various ocular disorders including *TIMP3 (*various
326   retinopathies[42]), *ABCA4* (Stargardt disease[12]), and *TYRP1* (oculocutaneous albinism[43]),
327   were found to be significantly differentially expressed by location.
328
329   Differential expression of particular transcription factors, including neural retina- and
330   RPE/choroid show conserved patterns of expression between macaque and human datasets, with
331   *IRX2* being upregulated in the macula. Other differentially expressed transcription factors that
332   show conservation with past human studies include *FOXI3*, which is upregulated in the
333   periphery, and *POU4F2*, *POU4F1*, as well as its target, *RIT2*, all of which are enriched in the
334   macula in both monkey and human datasets[7]. Additional transcription factors following similar
335   gene expression patterns across species in the RPE/choroid include *VEZF1* and *NR2F1*, which
336   are thought to be involved in retinal and vascular development[44, 45]. Identifying conserved
337   location-specific transcription factors can provide insight into the regulatory landscape of the two
338   tissues and how they relate to patterns of differential gene expression. It may be inferred then,
339   that these changes in global gene expression across location and tissue, driven by distinct sets of
340   transcription factors, likely reflect location-specific cellular processes and interactions.
341
342   Beyond patterns of transcriptional regulators, location-based tissue-tissue interactions are also
343   indicative of specific pathways being up- or downregulated by location, suggesting specific roles
344   in different locations of the tissues. The enrichment for Wnt signaling in kidney disease in the
345   downregulated interactions in the macula may be connected to the GO enrichment for renal

346   development in the RPE/choroid. Furthermore, ErbB signaling and peptide G-protein coupled
347   receptor signaling are required for retinal development, with ErbB involved in neural crest
348   development and adult pigment formation[46] and GCPR signaling involved in light processing
349   in photoreceptors[47]. The tissue-tissue interaction analysis suggests these pathways are
350   upregulated in the peripheral tissues of the eye. Certain pathways were enriched for tissue-tissue
351   interactions both up- and downregulated in the macula, including Hippo signaling. Hippo-YAP
352   signaling is known to play roles in both ocular development as well as disease, as it regulates
353   retinogenesis, photoreceptor cell differentiation, and retinal vascular development, but
354   misregulation also has associations with coloboma and optic fissure closure, uveal melanoma,
355   and retinal degeneration[48]. The widespread enrichment of this pathway informs the many roles
356   it plays in regulating the retinal landscape across location.
357
358   The three-way comparison of single cell, bulk human, and Rhesus macaque data showed many
359   more differentially expressed genes detected in our macaque dataset than the other two
360   sequencing methods. Furthermore, identifying differentially expressed genes in the Rhesus
361   monkey data that intersect with the single cell data allows us to identify known RPE-specific
362   genes that are conserved between the datasets including VIM[39], and PMEL[49], which we
363   have shown to change contiguously by location. Of the three macula-enriched genes in the
364   overlapping set, CXCL14 and WFDC1 have been previously identified as enriched in the macula
365   compared to peripheral retina via RNA microarray[50], and WFDC1 enrichment in the macula
366   was independently confirmed by both expression and immunostaining[51]. As such, our data
367   shows the known macula-enrichment of WFDC1 to be conserved. As a serine protease inhibitor,
368   mediator of endothelial cell migration and promoter of angiogenesis, its enrichment in the RPE
369   and specifically, the macula, may suggest a role for WFDC1 in age-related macular degeneration
370   [52], in which neovascularization beneath the macula is characteristic[50].
371
372   Considering the differential gene expression patterns across contiguous regions of the neural
373   retina and especially the RPE/choroid allows for a combined approach in which we assessed the
374   drivers of change as well as gross changes in gene expression by location. We identified highly
375   enriched gene ontologies associated with each tissue location and layer, highlighted sets of
376   contiguously changing transcription factors, determined important tissue-tissue interactions that
377   highlight various up- and down-regulated location-specific pathways, and examined the
378   conservation of gene expression patterns across multiple independent studies. In addition to the
379   previous RNA-sequencing studies performed on human and non-human primate retinas, the data
380   and findings presented here provide valuable resources for future studies aimed at identifying
381   regional specialization of the retina and understanding disease mechanisms.
382

390

391 **Table 1.** A summary of the differential gene expression (padj < 0.05) in retina and RPE/choroid
392 by location.

Tissue	Location	# Genes
Retina	Fovea	6,921
	Perimacula	6,926
	Periphery	10,517
	Fovea vs Perimacula	4,633
	Fovea vs Periphery	9,644
RPE/Choroid	Fovea	6,775
	Perimacula	7,465
	Periphery	10,983
	Fovea vs Perimacula	414
	Fovea vs Periphery	7,925

393
394 **Table 2.** Ligand-Receptor interactions across neural retina and RPE/choroid in the macula.

Upregulated Interactions in the Macula		Downregulated Interactions in the Macula	
RPE/Choroid	Neural Retina	RPE/Choroid	Neural Retina
NOTCH2	JAG2	EPHB2	EFNB1
FGFR1	NCAM1	WNT2B	FZD4
NTF3	NTRK3	EFNA1	EPHA2
IGF2	IGF1R	EPHB1	EFNB1
EPHA2	EFNA3	CCR1	CCL26
NOTCH1	JAG2	NRG2	ERBB3
PLXNB2	SEMA4D	CD48	CD244
NTF3	NTRK2	FLT3	FLT3LG
TNFSF10	TNFRSF10D	DSC1	DSG2
EPHA3	EFNA3	EFNA1	EPHA3
TEK	ANGPT1	PTPRC	CD22
VEGFA	FLT1	CCR5	CCL8
PLXNB2	SEMA4G	LGALS9	HAVCR2
NOTCH3	JAG2	MDK	ALK
WNT1	FZD1	PLXNC1	SEMA7A
NRP1	VEGFA	ANXA1	FPR2
EGFR	EGF	FGFR1	NCAM1
EPHA4	EFNB1	CCR1	CCL26
NRP2	SEMA3C	NGF	NTRK1
ERBB4	HBEGF	CD48	CD244
IGF2	IGF2R	FZD7	WNT3
EFNA1	EPHA2	CCR6	CCL20
EPHB1	EFNB1	CCR2	CCL26
TNF	TNFRSF1A	CCR2	CCL8

IGF2	IGF2R	PLXNB2	SEMA4C
EFNA3	EPHA4	PVR	CD96
CD55	ADGRE5	NRG1	ERBB4
CD44	SELE	ERBB3	NRG1
ERBB4	NRG4	PTPRC	CD22
CADM3	CADM1	SEMA5A	PLXNB3
EFNA1	EPHA3	CSF1R	IL34
CADM3	EPB41L1	CCR5	CCL8
VEGFA	FLT1	PDCD1	PDCD1LG2
VEGFA	KDR	CCR1	CCL8
NRP2	PGF	EREG	ERBB4
DPP4	CXCL12		
EPHB6	EFNB1		
NRP2	VEGFA		
FLT1	PGF		
EFNA1	EPHA4		
NRP2	SEMA3F		

Figure 1. (A) A volcano plot depicting differentially expressed genes between foveal and peripheral tissues in the neural retina. Colored genes show significant up- or down- regulation with several labeled genes having known tissue-specific roles in development and disease including PDE6B. (B) A volcano plot showing RPE fovea vs periphery differential expression, with key genes labeled, including ABCA4 and TIMP3. (C) Unfiltered differential expression analysis of contiguously changing genes from fovea to perimacula to periphery in the RPE/choroid exhibits distinct blocks of lowly expressed genes in the fovea with a progressive increase in expression in peripheral tissues as well as blocks of genes with progressive downregulation moving outwards through the tissue despite less obvious morphologic changes in the tissue as compared to neural retina. (D) Top 10 enriched gene ontology (GO) terms from the RPE/choroid differentially expressed gene set include cell junction organization and epithelial cell development. VEGF is enriched in multiple of these ontologies and has increased expression in the macula over the periphery. (E) A subset of genes identified as differentially expressed transcription factors by location in the RPE/choroid. Changes in transcriptional regulators can be a factor in driving gene expression changes. *These transcription factors have published associations with the respective tissue in the literature.
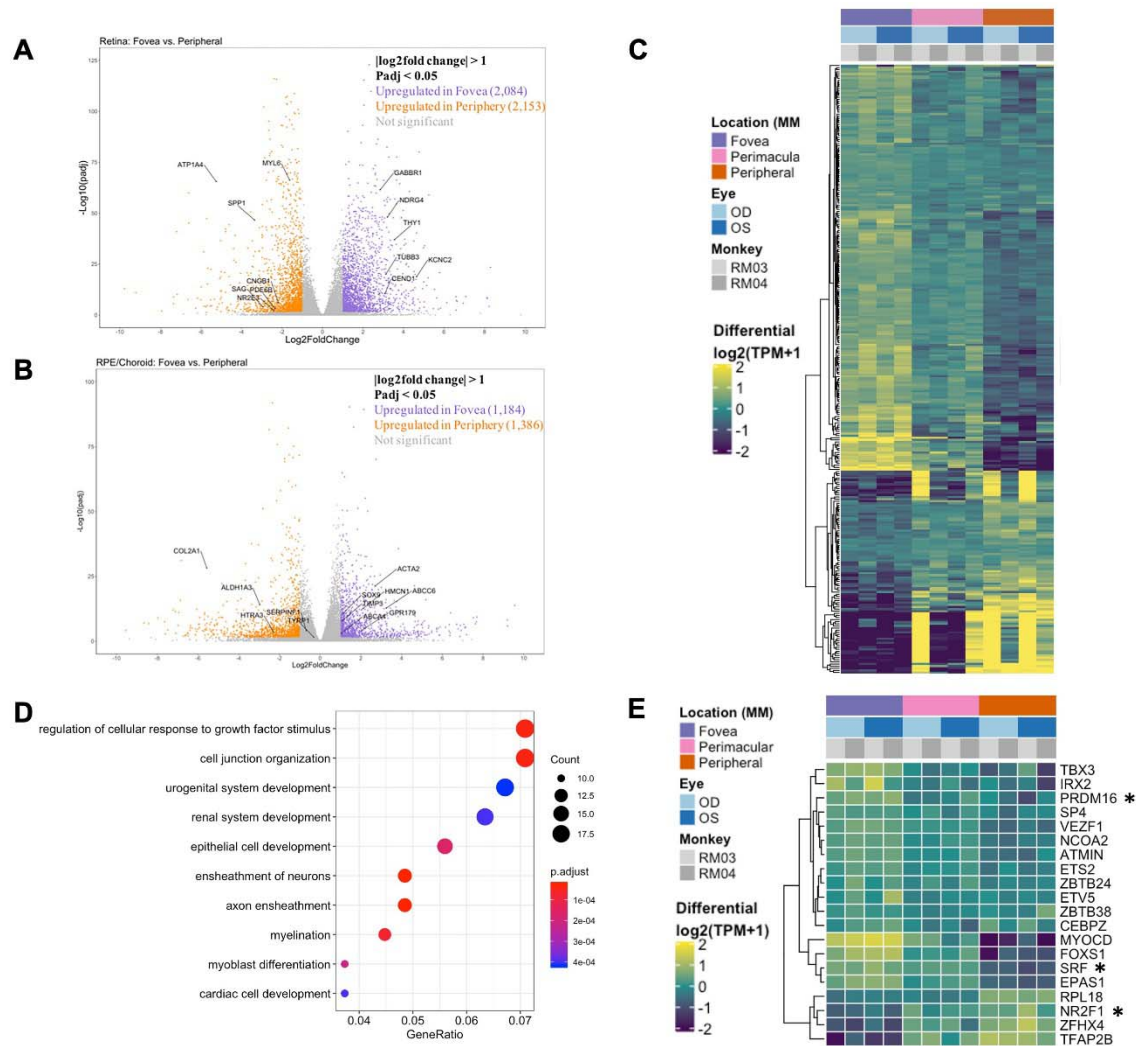
Figure 2. Tissue-tissue interactions showing receptor/ligand pairs in the central retina. (A) Upregulated macular receptors in the RPE/choroid are linked to their upregulated ligand in the macular neural retina. Interactors are grouped by signaling pathway and the width is scaled by average log2 fold change. (B) Downregulated macular receptors in the RPE/choroid and their respective downregulated ligand in the macular neural retina. (C) Upregulated macular ligands in the RPE/choroid are linked to their upregulated receptor in the macular neural retina. (D) Downregulated macular ligands in the RPE/choroid and their corresponding downregulated receptors in the macular neural retina.
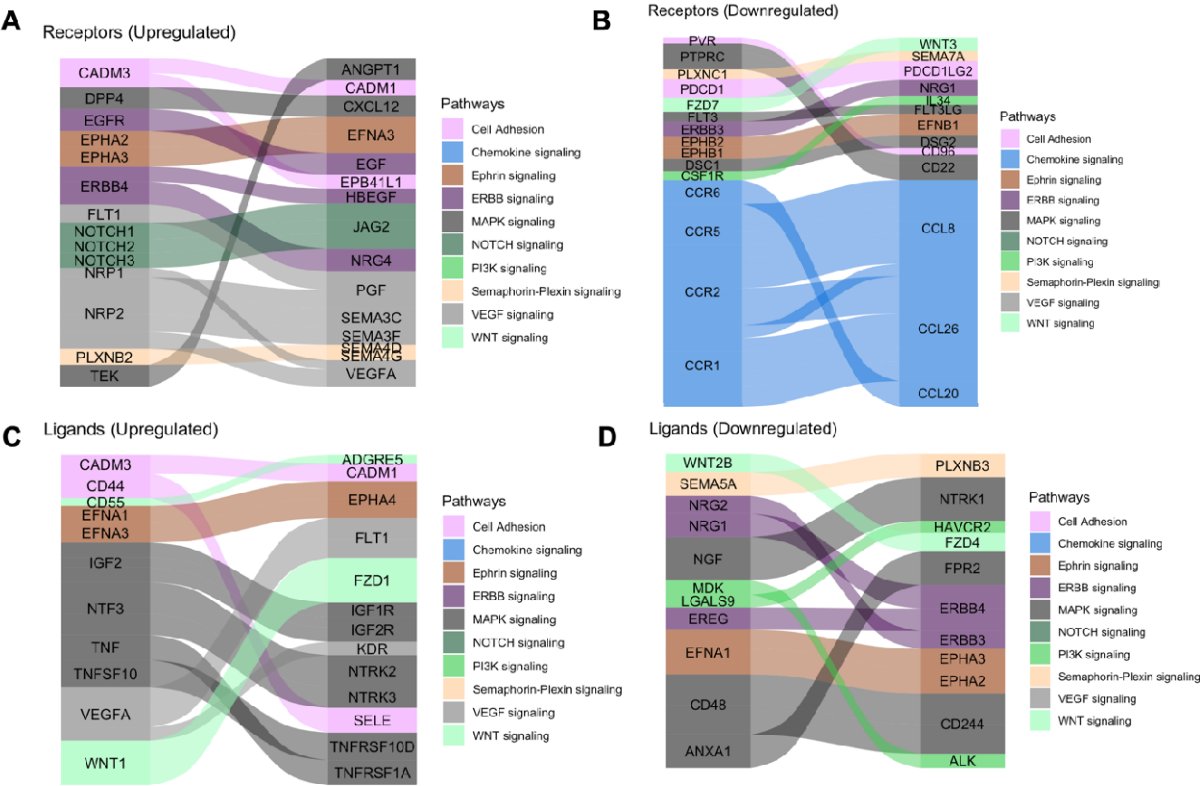
Figure 3. (A) Heatmap displaying the comparison of differential gene expression in the neural retina between published data from a human macula vs periphery set (Li et al., 2014, Whitmore et. al, 2014) and the macaque data presented here, with 664 genes following similar expression patterns. (B) A comparison of conserved differential expression to the human studies in the RPE/choroid tissue. Fewer genes follow similar patterns of differential expression. (C) GO enrichment for conserved differentially expressed genes between human and macaque datasets in the neural retina. Terms including neuronal connectivity and cellular morphogenesis are highly enriched.
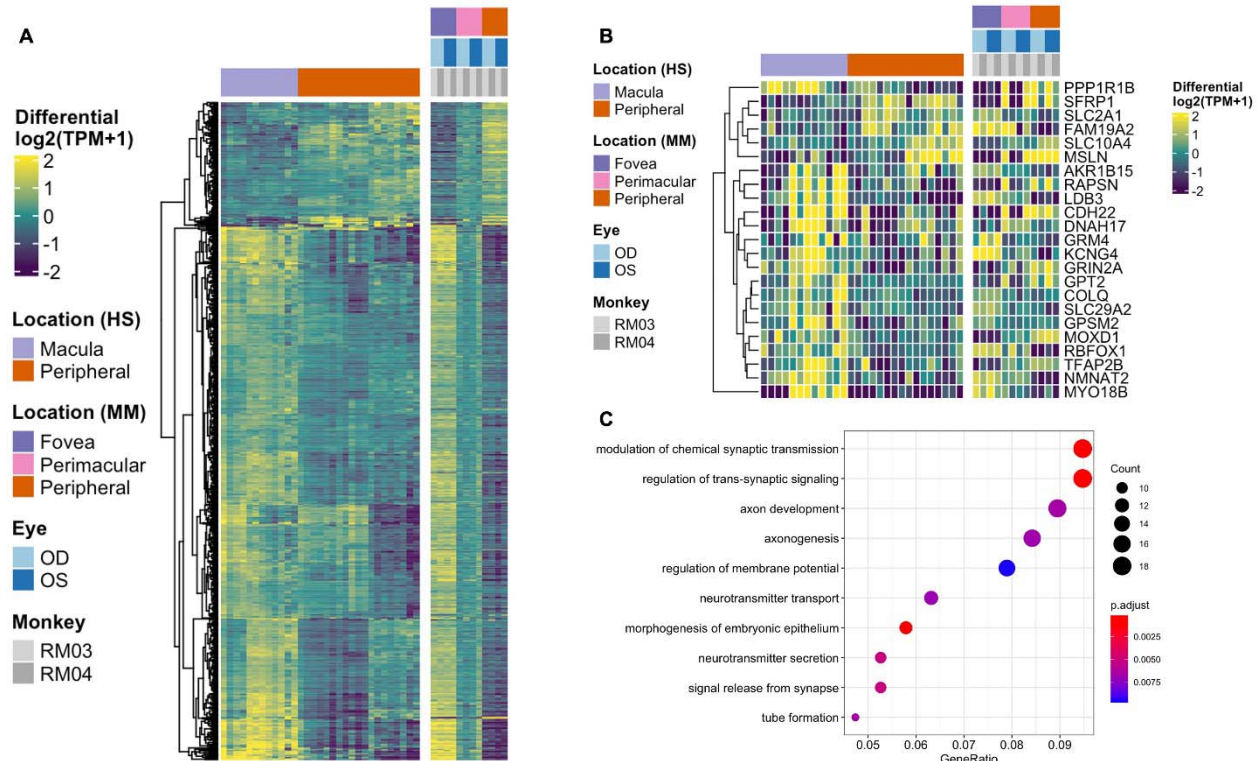
437
438 **Figure 4. (**A) Venn diagram of overlaps between differentially expressed genes between the
439 fovea and periphery in three systems: human single cell RPE, bulk human RPE-choroid, and
440 bulk macaque RPE-choroid. (B) Violin plot of the single cell expression with the ten genes
441 which overlap between the human single cell RPE testing and bulk macaque RPE-choroid
442 testing. (C) Heatmap of the same ten genes in our macaque RPE-choroid punches.
443
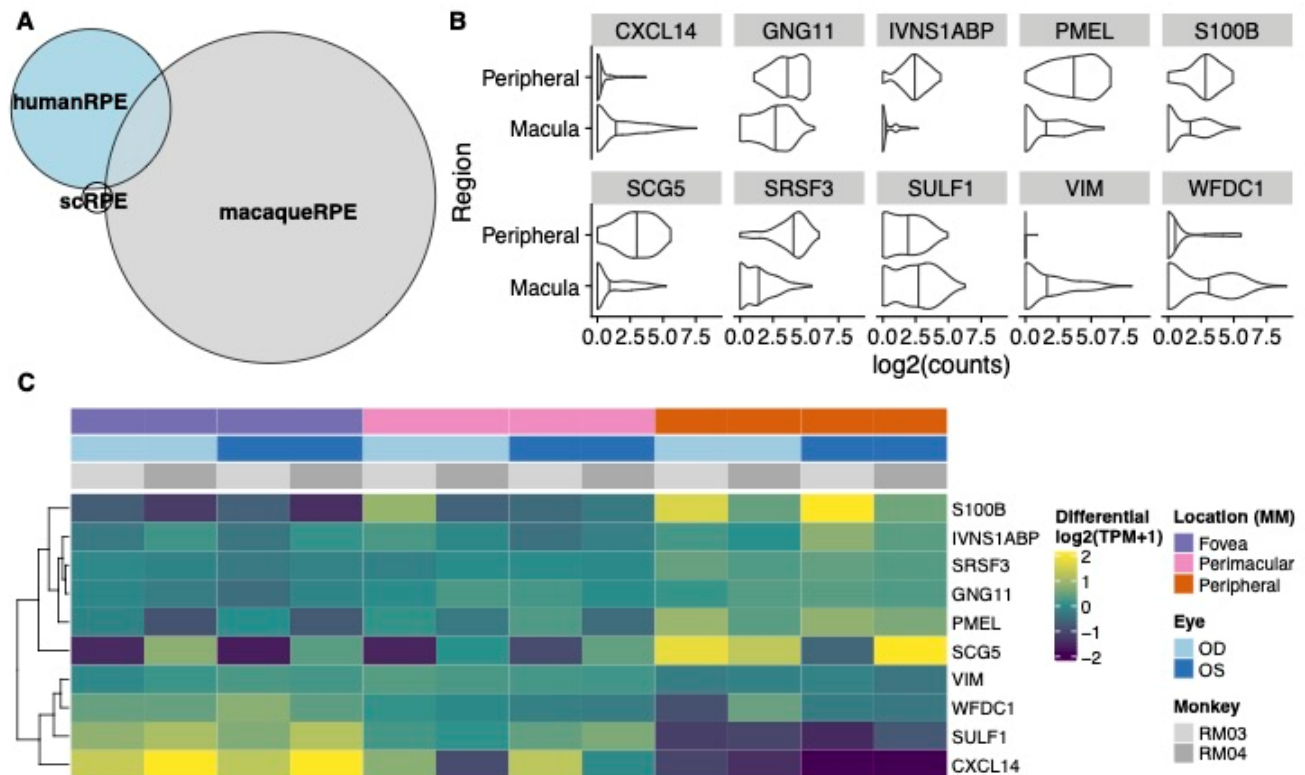
Supplemental Data

Figure S1. (A) Layout of punch biopsies taken from the Rhesus monkey eyes, including foveal (F), perimacular (PM), and peripheral (P) samples. (B) Diagram of the retina, highlighting the cell types in the neural retina as well as the RPE and choroid tissues (made in Biorender).
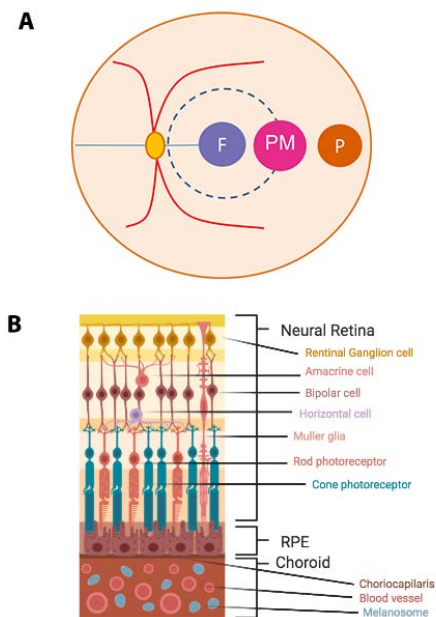
450
Figure S2. PCA clustering for the 1000 most variable genes sequenced. (A) Samples primarily
cluster by tissue type, with RPE/choroid samples clustering away from retina samples. (B)
Within the retina and RPE/choroid, foveal and peripheral samples tend to cluster furthest apart
with perimacular samples clustering less tightly between.
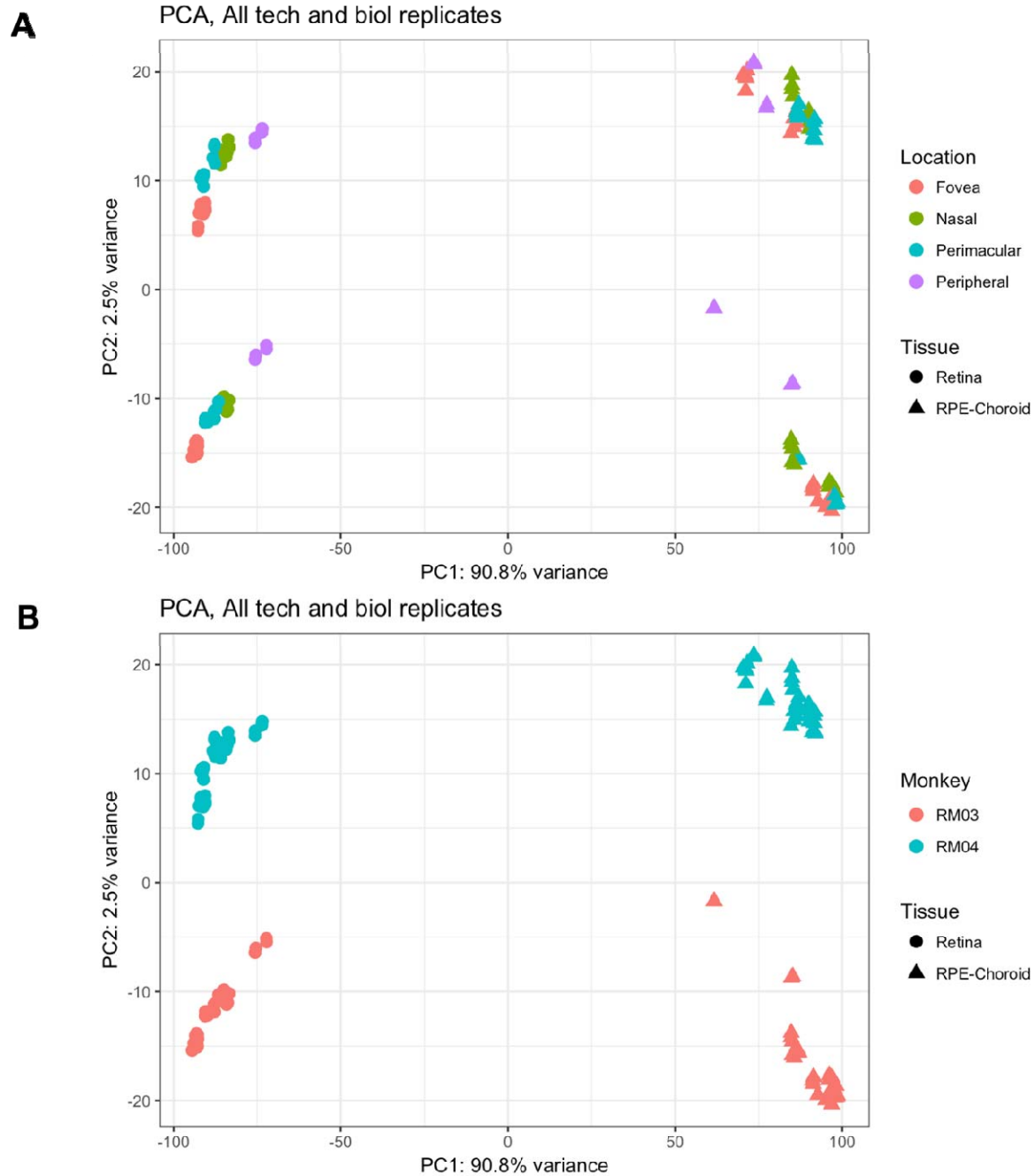
455
456 **Figure S3.** (A) Heatmap depicting macaque expression of published rod-enriched gene
457 expression (Holt et. al 2015, Mustafi et. al, 2016) across the neural retina reflects cellular
458 composition of rods in the retina. Genes are highly expressed in the periphery, where rod
459 composition is highly enriched, and lowly expressed in the fovea/macular which is highly cone-
460 enriched. (B) Peripheral and perimacular retinal samples express rod-enriched genes at a 2.8- and
461 1.7-fold increase compared to foveal retinal samples. The periphery is 1.6-fold enriched in cone
462 signal compared to the fovea in the neural retina (Table S1). (C) Changes in rod- and cone-
463 enriched gene expression do not vary greatly by location in RPE/choroid.
464
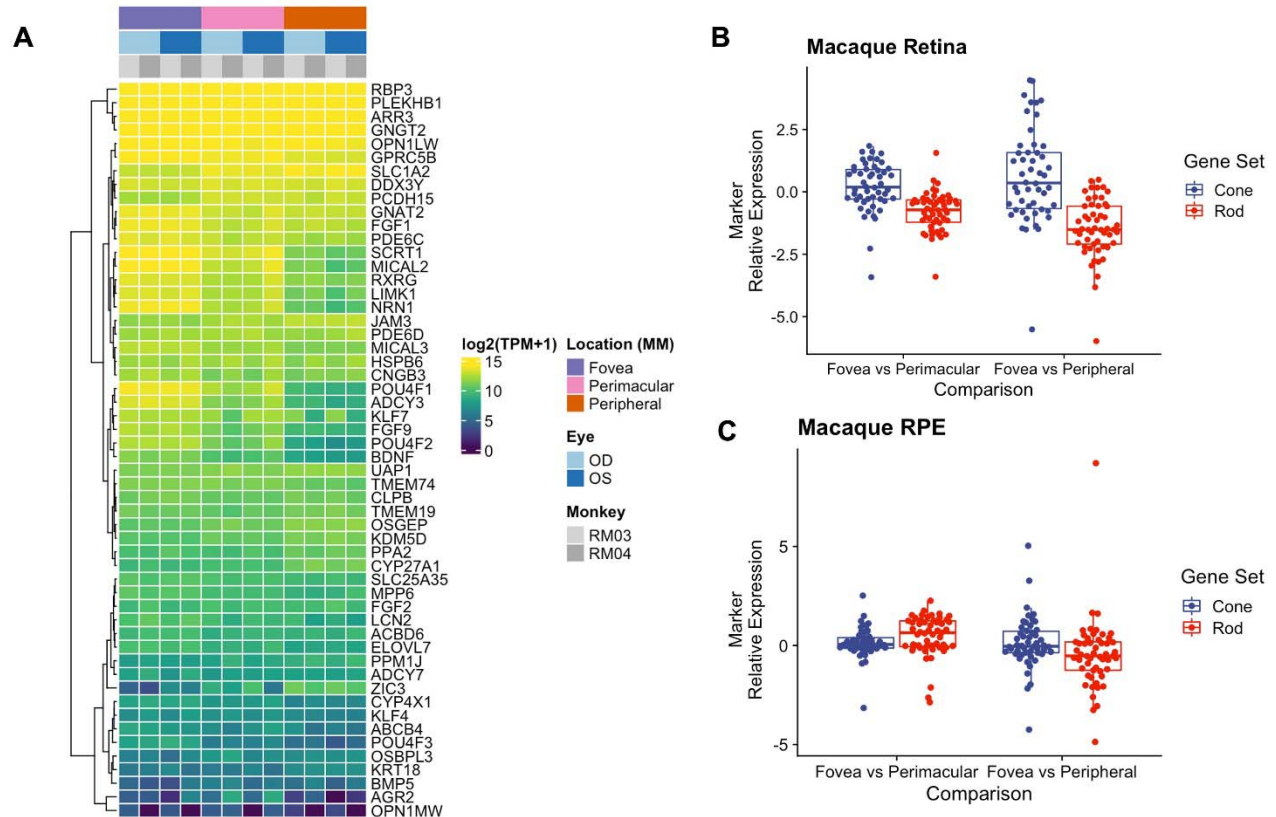
465
466
467 **Figure S4.** (A) Heatmap showing contiguous differential expression across location of the neural
468 retina tissue, also exhibiting distinct blocks of progressive up and down regulated gene
469 expression as seen for RPE/choroid in Fig. 1C. (B) A subset of genes identified as differentially
470 expressed transcription factors by location in the neural retina. Changes in transcriptional
471 regulators can be a factor in driving gene expression changes.
472 *These transcription factors have published associations with the respective tissue in the
473 literature. (C) Top 10 enriched gene ontology (GO) terms from the retina differentially expressed
474 gene set, including neuron projection, axon development, regulation of cell morphogenesis, and
475 protein localization and transport.
476
477
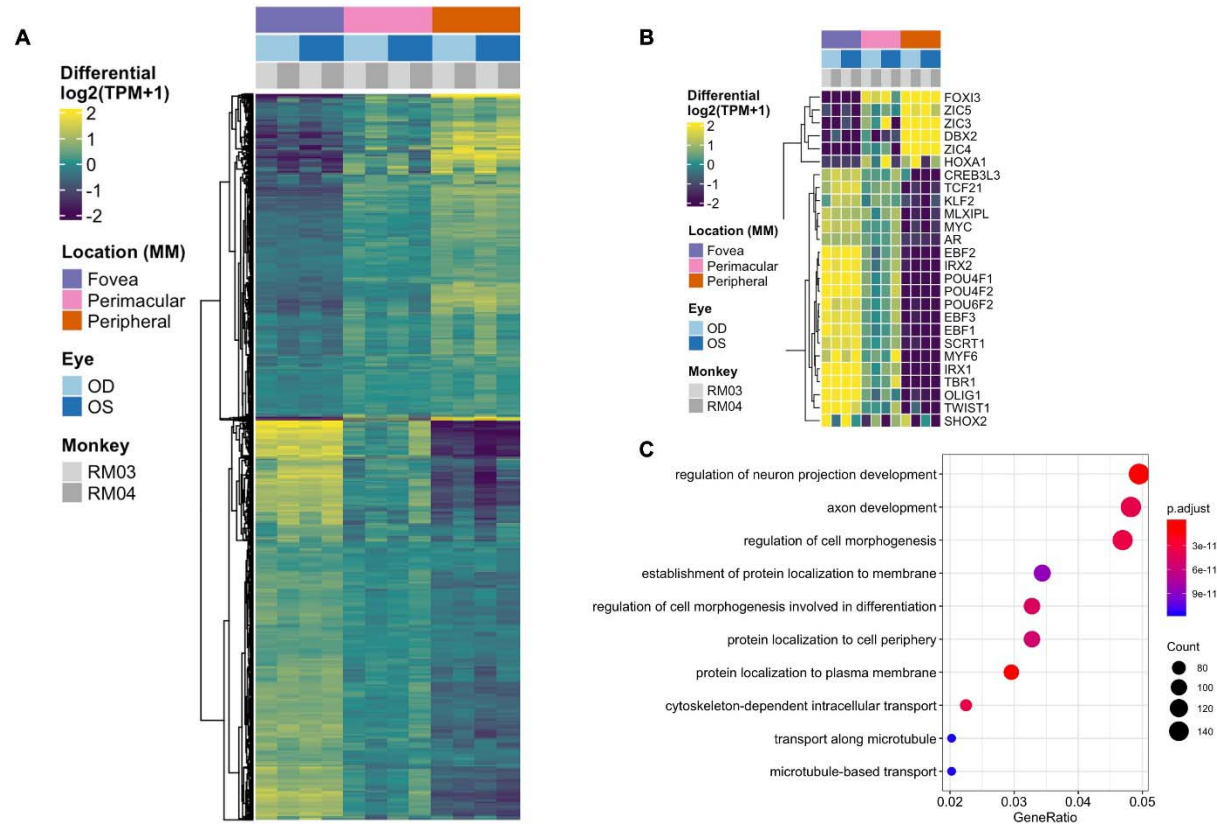
478
479
480
481 **Figure S5.** (A) Expression of commonly expressed transcription factors between the neural
482 retina and the RPE/choroid. While *NR2F1* and *IRX2* follow similar expression patterns across
483 location, *ZFHX4* actually displays opposite expression patterns in the retina and RPE/choroid
484 tissues. (B) Expression of these three transcription factors from the publicly available
485 EyeIntegration database (Swami and McGaughey et al., 2019) showing similar expression levels
486 of each gene in both tissue types with whole blood for comparison.
487
488
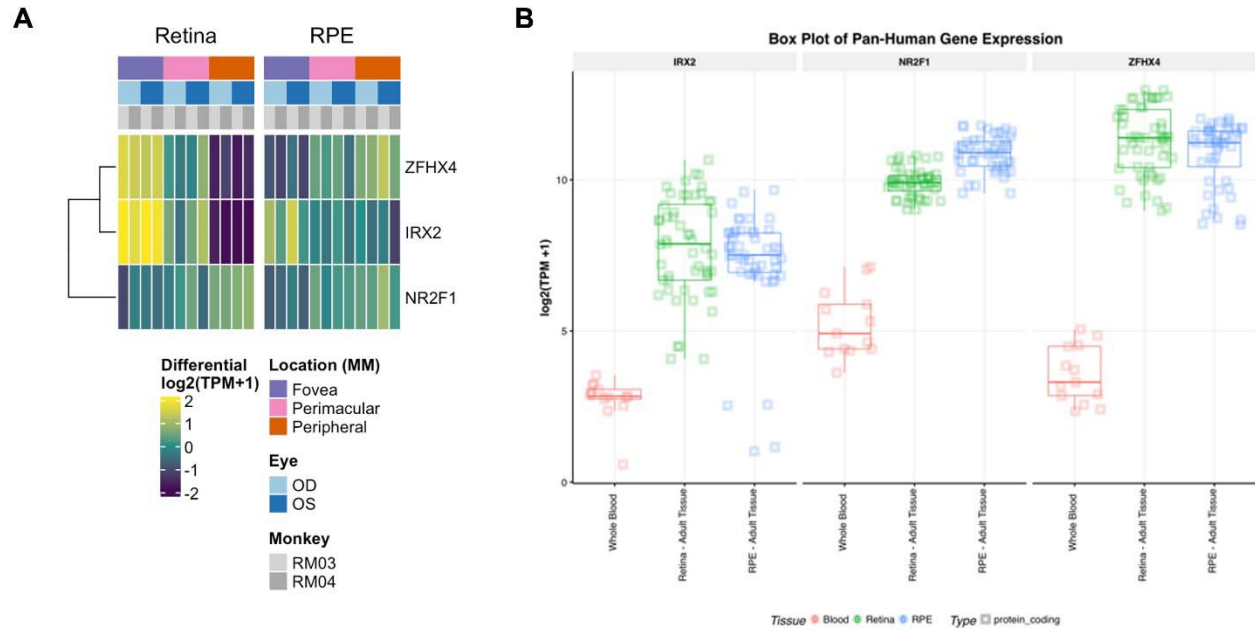
489
490
491
492
493 **Figure S6.** (A) A comparison of conserved transcription factor differential expression in the
494 neural retina between published data from a human macula vs periphery set (Li et al., 2014,
495 Whitmore et. al, 2014) and the macaque data presented here. (B) A similar comparison of human
496 conservation of transcription factor differential expression in the RPE/choroid tissue. (C) Top
497 enriched GO terms for the conserved gene expression across fovea to periphery in the
498 RPE/choroid. Top terms include regulation of neurotransmitter levels and metabolic processes as
499 well insulin secretion.

500

501
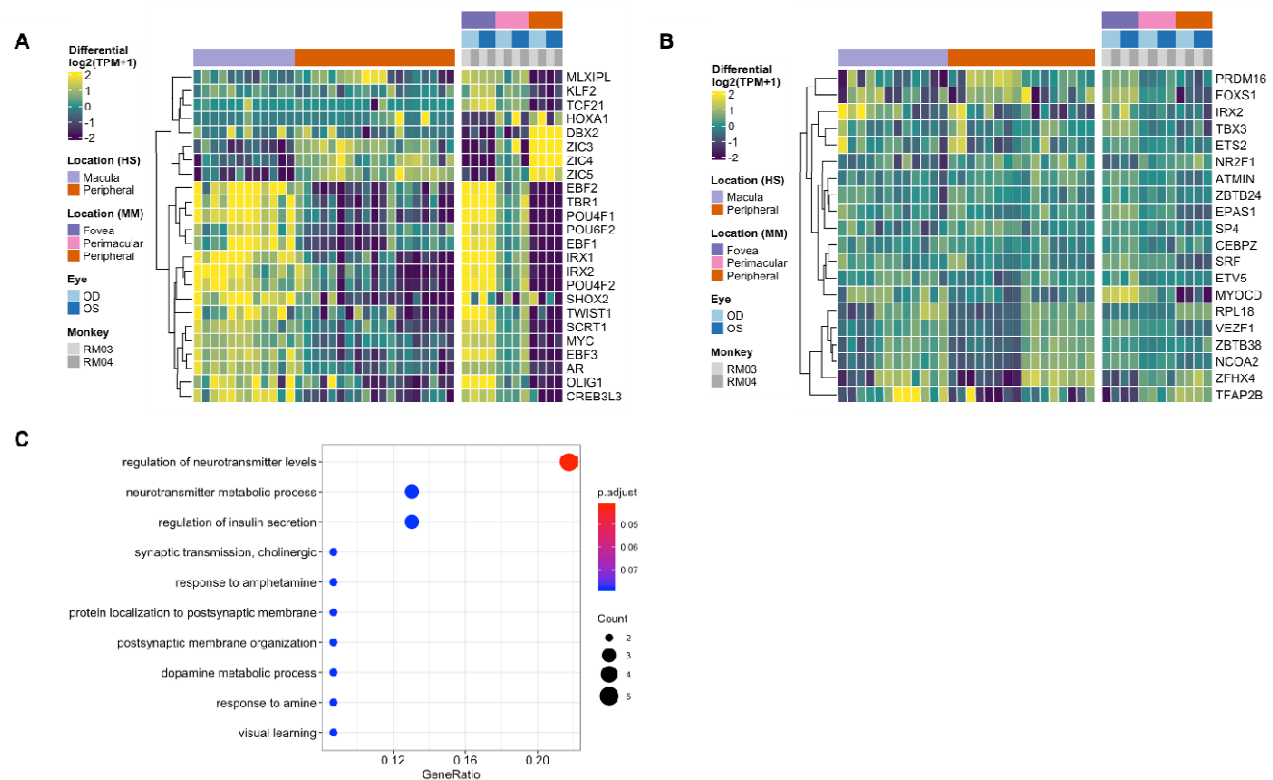
Figure S7. (A) Enrichr bar graph depicting highly enriched pathways via the WikiPathways 2019 Human database for the downregulated ligand/receptor interactions in the macula. Top enriched pathways include Wnt signaling in kidney diseaseand ErbB signaling. (B) Enrichr clustergram depicts the genes contributing to the enriched pathway terms including *WNT*, *FZD4*, and *ERBB3*. (C) Enrichr bar graph for upregulated ligand/receptor interactions in the macula. Top enriched pathways include PI3K-Akt signaling and Focal Adhesion-PI3K-Akt-mTOR, both of which are involved in the VEGF signaling pathway. (D) Enrichr clustergram is enriched for genes including *VEGFA*, *FLT1*, and *KDR*, all of which are key components of VEGF signaling.

510

511
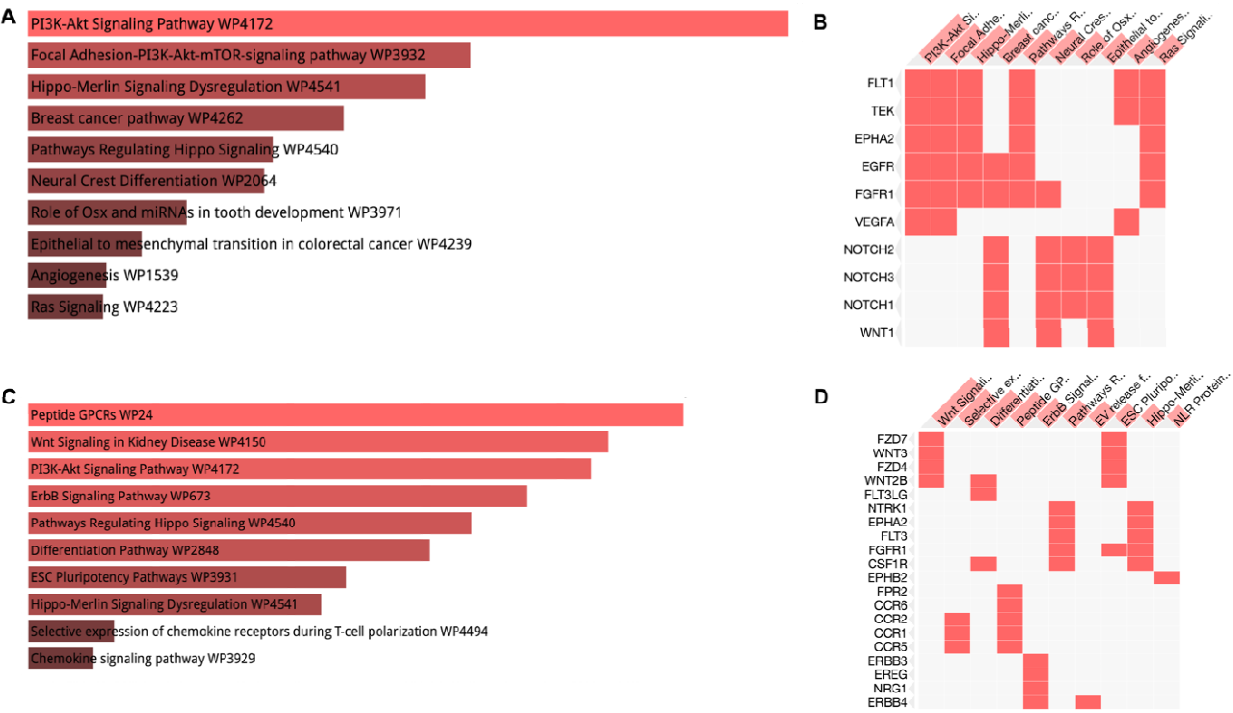
512
513
514
515
516
517
518
519
520 **Table S1.** Rod- and Cone-Enriched gene expression in Retina and RPE/choroid compared across
521 location

Tissue	Comparison	GeneSet	estimate	enrichment	statistic	p.value	parameter	conf.low	conf.high
Retina	Fovea vs Perimacular	Rod	-0.7821306	-1.7196686	-7.4071987	1.11E-09	52	-0.9940137	-0.5702476
Retina	Fovea vs Peripheral	Rod	-1.4620671	-2.7550282	-8.9989078	3.48E-12	52	-1.7880902	-1.1360439
Retina	Fovea vs Perimacular	Cone	0.20531647	1.15293923	1.46077663	0.15045974	49	-0.0771353	0.48776821
Retina	Fovea vs Peripheral	Cone	0.6492966	1.56840332	2.441338	0.01829112	49	0.11483133	1.18376187
RPE	Fovea vs Perimacular	Rod	0.47748612	1.39231546	3.3946687	0.00132244	52	0.1952359	0.75973635
RPE	Fovea vs Peripheral	Rod	-0.4613632	-1.3768422	-1.8370341	0.07192272	52	-0.9653239	0.0425975
RPE	Fovea vs Perimacular	Cone	0.13785476	1.10026784	1.27906465	0.20689857	49	-0.0787328	0.35444235
RPE	Fovea vs Peripheral	Cone	0.14454836	1.10538455	0.76617502	0.44724757	49	-0.2345828	0.52367948

522

523 **Table S2.** List of conserved genes between human and macaque data as seen in the heatmap
524 (Fig. 3A)

AACS	CCDC88C	ELOVL6	IFT22	MTA2	POLR2G	SHKBP1	TMEM189
ABCA1	CCDC92	EMB	IGIP	MTMR4	POPDC3	SHOX2	TMEM246
ABCG1	CCER2	EMC8	IK	MTURN	PPARG	SIAE	TMEM26
ABHD10	CCM2	EML4	IKBKE	MVD	PPIF	SIAH2	TMEM37
ABHD17A	CCNYL1	ENDOD1	IKBKG	MX1	PPM1K	SIGMAR1	TMEM41A
ABHD6	CD109	ENOX1	IL17RD	MYADM	PPP1R12C	SIRT5	TMEM71
ABR	CD151	ENPP1	IL17RE	MYB	PPP1R1C	SIX2	TMEM97
ACACA	CD274	ENTPD3	INCENP	MYC	PPP1R3C	SLC15A3	TMOD2
ACAT2	CD4	EPB41L1	INF2	MYCBP2	PPP1R3D	SLC16A7	TMTC1
ACER3	CD5	EPB41L2	INHBA	MYLIP	PPP2R2C	SLC16A9	TNFAIP2
ACLY	CD8A	EPB41L3	INPP4A	MYO1C	PPP2R5B	SLC22A18	TNFRSF21
ACOT7	CDC42BPA	EPDR1	INPP4B	MYO5A	PPP3CB	SLC25A1	TNFSF13
ACOX2	CDCA2	EPHA2	INPP5A	MYO5C	PRCP	SLC25A12	TNIP1
ACSS2	CDCA7	EPHA4	INPP5F	MYO6	PRDM11	SLC25A40	TOB2
ACTL6A	CDK14	EPHA5	INPP5J	MYOM1	PRDM4	SLC25A46	TPBG
ACTR1A	CDK18	EPHX4	INSIG1	NAALADL1	PRDX5	SLC26A11	TPGS2
ACTR1B	CDK6	ESYT1	IQCA1	NACAD	PRELP	SLC2A13	TRAF3IP2

ADAM23	CDKN2D	ETFBKMT	IQCK	NACC2	PREPL	SLC2A6	TRAF5
ADAMTS2	CDR2L	ETHE1	IQSEC3	NAGA	PRICKLE1	SLC35D1	TRAPPC1
ADAMTS7	CDS2	EXOC1	IRS1	NANS	PRIMA1	SLC36A1	TRHDE
ADAMTSL2	CDYL2	EXOSC5	IRX1	NAP1L2	PRKAG2	SLC39A13	TRIM2
ADAP1	CELSR1	EXPH5	IRX2	NAP1L4	PRKCB	SLC39A8	TRIM24
ADCY3	CEP68	F7	IRX3	NAP1L5	PRKG2	SLC41A3	TRIM37
ADD2	CERS2	FABP3	ISCU	NARS	PRPH	SLC45A1	TRIP4
ADGRA2	CFAP298	FAM102B	ISLR2	NBEAL2	PRRT2	SLC47A2	TRIP6
ADGRA3	CFI	FAM104A	ISYNA1	NCDN	PRRT3	SLC4A3	TRMT2B
ADI1	CFL2	FAM110B	ITGB1BP1	NCS1	PRSS16	SLC6A15	TRPC3
ADIPOR1	CHD3	FAM111A	ITPK1	NDEL1	PRUNE2	SLC6A17	TRPM2
ADRA2A	CHD7	FAM120AOS	JAK1	NDRG2	PSD3	SLC9A1	TRPM4
ADRB2	CHIC1	FAM124B	JAKMIP2	NDRG4	PSD4	SLC9A6	TRPS1
ADSS	CHRAC1	FAM131A	JHY	NDUFA4L2	PSIP1	SLCO2A1	TRPV2
ADSSL1	CHRDL1	FAM131B	KANK3	NEBL	PSMA7	SLCO3A1	TSC22D3
AFAP1	CHST9	FAM189A2	KCNA2	NECAP2	PSMD1	SMARCC1	TSPAN2
AFF3	CIAPIN1	FAM189B	KCNAB2	NEDD4L	PTDSS1	SMIM10	TSPAN31
AGBL5	CIC	FAM198B	KCNC2	NEFH	PTH1R	SMIM12	TSPAN9
AGO1	CISD1	FAM210B	KCNK1	NEFL	PTMS	SMOC1	TSPYL4
AGPAT2	CIT	FAM219A	KCNN2	NEFM	PTPN3	SMYD2	TTC39A
AHNAK2	CLCN5	FAM43A	KCNQ3	NEK6	PTPRE	SMYD3	TTC39B
AHR	CLCN6	FAM49A	KCNQ4	NEPRO	PTPRN2	SNAPC2	TTC39C
AIF1L	CLDN1	FAM53B	KCNQ5	NES	PTPRU	SNCA	TTC7B
AJUBA	CLDN2	FAM69A	KCTD17	NFATC1	PXYLP1	SNCAIP	TUBA1A
ALDH1B1	CLIC5	FAM69B	KCTD2	NFE2L1	PYGB	SNCG	TUBA1B
ALDH1L1	CLIP2	FAM69C	KCTD20	NFIB	PYGL	SNN	TUBB
ALKBH6	CLSTN2	FAM83G	KCTD21	NFIX	PYGM	SNRPD3	TUBB3
ALPK3	CLTC	FAM84A	KDM5B	NIPA1	QPRT	SNW1	TUBB4A
AMER1	CLTCL1	FAM98A	KIAA1324L	NIPAL2	QRFPR	SNX16	TUBGCP5
AMPD2	CLU	FAR2	KIF21A	NIPAL3	QRICH1	SNX9	TULP2
ANK1	CMAS	FASN	KIF3C	NKAPD1	QSOX1	SORBS2	UBASH3B
ANK3	CMC2	FAT1	KIF5A	NKD2	RAB11FIP4	SORL1	UBE2E2
ANKRD11	CMPK1	FBLL1	KIFAP3	NKRF	RAB11FIP5	SOX5	UBE2N
ANKRD13A	CNBP	FBLN1	KIFC2	NLRP1	RAB15	SP1	UBE2O
ANKRD13D	CNN3	FBRS	KLC1	NMNAT2	RAB33A	SPARCL1	UBE2T
ANKRD24	CNNM1	FBXO2	KLF13	NMRK2	RAB35	SPATA20	UBFD1
ANKRD27	CNOT2	FBXW5	KLF7	NOTCH4	RAB37	SPATS2	UBL4A
ANKRD40	CNST	FBXW7	KLF8	NOVA1	RAB3D	SPHK1	UCHL1
ANKRD50	CNTNAP1	FCHO1	KNDC1	NPHP1	RAB5B	SPINT1	UGP2

ANKRD52	COL11A1	FDPS	KREMEN1	NPR3	RAB6A	SPNS2	URM1
ANKRD9	COL14A1	FEZ1	KRI1	NPTN	RAB6B	SPOCK2	USB1
ANO4	COL18A1	FFAR1	L1CAM	NQO2	RAB8A	SPTB	USP14
ANO5	COL23A1	FGF10	LACC1	NRAS	RABGGTA	SPTSSB	USP25
ANXA11	COL2A1	FGF13	LAMA2	NRF1	RAC3	SQLE	USP31
ANXA6	COL3A1	FGFR1	LAMA4	NRN1	RAP2A	SREBF2	USP35
ANXA7	COL4A3	FHDC1	LARP1	NSG1	RARRES2	SRGAP2	USP5
AP1M1	COL4A4	FHL2	LATS2	NT5M	RASA3	SRPX	UTRN
AP2B1	COLCA2	FIGN	LDLR	NUAK1	RASGRP2	SSH3	UXS1
AP3M1	COPZ1	FKBP1B	LGALS1	NUDT10	RASGRP3	ST14	VAMP1
AP5S1	CORO1C	FKBP9	LGALS3	NUDT18	RASSF2	ST3GAL2	VANGL1
APBA1	CORO2A	FLOT1	LGALS8	NUDT3	RBFOX2	ST3GAL6	VAPB
APBA2	CORO2B	FLYWCH2	LGALSL	NUMBL	RBPMS	ST5	VASH1
APOBEC3C	CORO6	FMNL1	LGI2	NUP214	RBPMS2	ST6GAL1	VIM
APOD	COX4I2	FMO3	LGI3	NUP37	RCAN2	ST6GALNAC 2	VOPP1
APOE	CPEB1	FNBP1	LHFPL2	NUP93	RDH10	ST6GALNAC 5	VPS35
APOL2	CPED1	FNDC10	LIMK1	NXN	REEP1	ST8SIA4	VSIG10
APP	CPLX1	FNDC11	LIMS2	ODF3B	REEP5	STAC2	VSTM2L
AR	CPNE3	FOCAD	LIN7A	OGDH	RELL2	STARD13	VWC2
ARAF	CPNE9	FOXD1	LITAF	OPA1	REPS2	STARD4	WDR20
ARAP2	CPZ	FOXF2	LIX1L	OPLAH	RET	STAT4	WDR72
ARFGEF3	CREG1	FOXN3	LMO2	OPN3	RETREG1	STAT6	WDYHV1
ARFIP1	CRYAB	FRY	LNX1	OPTN	RFFL	STEAP4	WEE1
ARHGAP42	CRYL1	FXYD3	LPIN1	OSBPL10	RFLNA	STK32A	YAP1
ARHGAP44	CSDC2	FXYD6-FXYD2	LRFN5	OSBPL5	RFX5	STMN2	YBX1
ARHGAP6	CSNK1G3	GABBR1	LRP11	OXCT2	RGS6	STMN3	YWHAB
ARHGAP9	CSRP2	GALNT10	LRP2	OXR1	RGS7BP	STS	YWHAG
ARHGEF17	CTDSP1	GALNT9	LRP3	OXTR	RHNO1	SUCLG2	YWHAH
ARHGEF7	CTIF	GAREM2	LRPAP1	PADI2	RHOC	SULF2	ZBTB7C
ARL8B	CTNNAL1	GAS2L3	LRPPRC	PAFAH1B1	RHOD	SULT4A1	ZC2HC1A
ARMCX3	CTNNBIP1	GATB	LRRC36	PAFAH1B2	RHOF	SURF2	ZCCHC24
ARNT	CTNND2	GCNT4	LRRC4B	PAIP2B	RHOJ	SUSD1	ZDHHC23
ARPC2	CTSH	GCOM1	LRRC4C	PALM3	RIC8B	SV2C	ZDHHC3
ARRB1	CYB561	GDI1	LRRC8C	PALMD	RNASEH2B	SVEP1	ZDHHC5
AS3MT	CYB5A	GFOD1	LRRFIP1	PAM	RNF112	SYDE1	ZDHHC7
ASAP1	CYB5R3	GIPC2	LRRK2	PANK1	RNF121	SYN2	ZFAND3
ASAP2	CYFIP1	GLI3	LSS	PANX1	RNF144B	SYN3	ZFHX3
ATAT1	CYGB	GLRB	LUZP1	PANX2	RNLS	SYNGR3	ZFHX4

ATL1	DAP	GNA12	LYNX1-SLURP2	PAQR8	ROBO1	SYNJ2	ZFP92
ATOH8	DBNDD1	GNB1	MAD1L1	PARP16	ROBO2	SYNPO2	ZFYVE9
ATP10A	DCBLD1	GNG12	MAGEE1	PATJ	RPL11	SYS1	ZHX2
ATP13A2	DCDC2	GNG5	MAL	PBXIP1	RPL12	SYT11	ZNRF1
ATP1B1	DCTN1	GOLIM4	MAOB	PC	RPL22	SYT7	ZNRF2
ATP2B2	DCTN2	GOT1	MAP1A	PCBP2	RPL36	SYTL2	ZYG11B
ATP2B3	DDAH1	GPATCH1	MAP1B	PCDH9	RPL4	TACC3	
ATP8B2	DDHD2	GPC4	MAP3K20	PCDHB15	RPL41	TAF4B	
ATRNL1	DDR2	GPCPD1	MAP3K9	PCMT1	RPS6KA4	TAF6	
ATXN7L3	DEAF1	GPM6B	MAP4	PCNX2	RRAGA	TANC1	
B3GNT8	DESI1	GPR143	MAP4K4	PCYT2	RRAS2	TANGO2	
B3GNT9	DEXI	GPR161	MAP7D1	PDE4A	RREB1	TATDN3	
B4GALNT1	DGKA	GPRC5B	MAPK10	PDE8B	RRP1B	TBC1D30	
B4GALT5	DGKQ	GPX3	MAPK8IP3	PDLIM3	RTN1	TBC1D4	
BASP1	DHCR24	GPX8	MAPK9	PDLIM4	RTN3	TBC1D9B	
BBC3	DIP2C	GRB2	MAPRE2	PDP1	RUFY2	TBRG1	
BBS12	DISC1	GRK3	MARCH2	PDP2	RUNDC3B	TC2N	
BBS9	DKK3	GRSF1	MARCKS	PDXK	RUSC1	TCAF1	
BCAN	DLC1	GSK3B	MARF1	PDXP	RXRG	TCEAL7	
BCAS4	DLG1	GSTA4	MARK1	PDZD7	RYR2	TCF25	
BCL2	DMTN	GSTO1	MARVELD2	PERM1	S100A10	TCF7L2	
BCL2L11	DNAJC22	GTPBP1	MAST3	PERP	S100A13	TCIRG1	
BCL2L2	DNAJC27	GYG1	MCF2	PGM2L1	S100A16	TCTN1	
BDNF	DNM1L	GZMK	MCF2L	PGRMC2	SACM1L	TCTN3	
BEAN1	DOCK11	H2AFY	MCTP1	PHACTR3	SACS	TEDC2	
BHMT2	DOCK5	H3F3B	MDH1	PHF12	SAE1	TENM3	
BICD2	DOK7	HABP4	MDK	PHF24	SAMD14	TESC	
BLOC1S2	DPYS	HADHB	MED8	PHLDA2	SBF2	TEX261	
BLVRB	DPYSL2	HAGHL	MEI1	PHOSPHO1	SBSPON	TFCP2	
BMPR1B	DSG2	HARS	MESD	PI16	SC5D	TFCP2L1	
BRSK1	DSP	HBEGF	METTL7B	PI4KA	SCAMP3	TGFB1I1	
BTD	DTNB	HECA	MFHAS1	PICK1	SCD	TGFBR3L	
C1QTNF1	DTX4	HECW2	MFSD6	PID1	SCG5	TGIF2	
CA2	DUSP14	HEPH	MGLL	PIEZO1	SCN1A	TGOLN2	
CA5B	DUSP3	HERC5	MGST2	PIK3CD	SCN1B	THAP10	
CABLES1	DYNC1H1	HERPUD2	MGST3	PIP4K2A	SCN8A	THEM6	
CABLES2	DYNC1I1	HES6	MICAL2	PITHD1	SCUBE2	THY1	
CACFD1	DYNC1LI1	HEY2	MICAL3	PITPNC1	SDHA	TICAM1	
CACNA2D3	DYNC1LI2	HINT1	MICU1	PITX2	SEC23B	TIFA	

CACNB3	DYNLL2	HMGCR	MIGA2	PKHD1	SELENBP1	TIGD2	
CALM3	DYNLT3	HMOX2	MITF	PLA2G4A	SEMA6D	TIMP4	
CAMK1	DYSF	HNRNPC	MLLT11	PLCB1	SEPT3	TJP2	
CAMKK2	E2F5	HOPX	MLPH	PLCL2	SEPT5	TLL1	
CAMTA2	EBF1	HPGD	MMP15	PLD1	SERINC5	TLR3	
CAP2	EEF1AKMT3	HPS1	MOAP1	PLEKHA6	SERP2	TM6SF1	
CAPNS1	EFEMP2	HR	MPP1	PLK2	SERPINE2	TMC6	
CASP2	EFR3B	HSD17B11	MPP3	PLS3	SFRP2	TMED4	
CAST	EFS	HSP90AB1	MPST	PLSCR4	SFXN1	TMEM106C	
CAV1	EGFL7	HSPA12A	MRFAP1	PLVAP	SGCD	TMEM120A	
CAV2	EIF2AK2	HTR1B	MRFAP1L1	PLXDC2	SGF29	TMEM123	
CAVIN1	EIF4EBP1	HTR1F	MROH1	PMEPA1	SGSH	TMEM131L	
CBFB	EIF5A2	HYAL3	MRPS15	PNMA3	SH3BGRL2	TMEM144	
CBLN3	ELAVL2	ICA1	MRVI1	POC5	SH3BGRL3	TMEM150C	
CCDC191	ELAVL3	ID3	MSI2	PODXL	SH3GLB2	TMEM159	
CCDC69	ELAVL4	IDI1	MSL3	POFUT1	SH3RF1	TMEM179B	
CCDC85A	ELMO1	IFIT3	MSRB3	POLR2C	SHANK3	TMEM181	

525

526

References

528

529 1. Grover, S., et al., *Comparison of retinal thickness in normal eyes using Stratus and Spectralis optical coherence tomography.* Invest Ophthalmol Vis Sci, 2010. **51**(5): p. 2644-7.

532 2. Purves, D., et al., *Neuroscience 2nd edition. sunderland (ma) sinauer associates.* Types of Eye Movements and Their Functions, 2001.

534 3. Nickla, D.L. and J. Wallman, *The multifunctional choroid.* Prog Retin Eye Res, 2010. **29**(2): p. 144-68.

536 4. Bagci, A.M., et al., *Thickness profiles of retinal layers by optical coherence tomography image segmentation.* Am J Ophthalmol, 2008. **146**(5): p. 679-87.

538 5. Mori, K., J. Kanno, and P.L. Gehlbach, *Retinochoroidal Morphology Described by Wide-Field Montage Imaging of Spectral Domain Optical Coherence Tomography.* Retina, 2016. **36**(2): p. 375-84.

541 6. Holt, R., et al., *Identification of rod- and cone-specific expression signatures to identify candidate genes for retinal disease.* Exp Eye Res, 2015. **132**: p. 161-73.

543 7. Daiger, S., et al., *Data services and software for identifying genes and mutations causing retinal degeneration.* Invest Ophthalmol Vis Sci, 1998. **39**(S295).

545 8. Di Pierdomenico, J., et al., *Early events in retinal degeneration caused by rhodopsin mutation or pigment epithelium malfunction: differences and similarities.* Frontiers in neuroanatomy, 2017. **11**: p. 14.

548 9. Lamin, A., et al., *Changes in volume of various retinal layers over time in early and intermediate age-related macular degeneration.* Eye, 2019. **33**(3): p. 428-434.

550   10.   Jones, B.W., R.E. Marc, and R.L. Pfeiffer, *Retinal degeneration, remodeling and*
551   *plasticity.* 2018.
552   11.   MacDonald, I.M. and T. Lee, *Best vitelliform macular dystrophy.* 2013.
553   12.   Walia, S. and G.A. Fishman, *Natural history of phenotypic changes in Stargardt macular*
554   *dystrophy.* Ophthalmic genetics, 2009. **30**(2): p. 63-68.
555   13.   Li, M., et al., *Comprehensive analysis of gene expression in human retina and supporting*
556   *tissues.* Human molecular genetics, 2014. **23**(15): p. 4001-4014.
557   14.   Whitmore, S.S., et al., *Transcriptomic analysis across nasal, temporal, and macular*
558   *regions of human neural retina and RPE/choroid by RNA-Seq.* Experimental eye
559   research, 2014. **129**: p. 93-106.
560   15.   Peng, Y.-R., et al., *Molecular classification and comparative taxonomics of foveal and*
561   *peripheral cells in primate retina.* Cell, 2019. **176**(5): p. 1222-1237. e22.
562   16.   Voigt, A., et al., *Molecular characterization of foveal versus peripheral human retina by*
563   *single-cell RNA sequencing.* Experimental eye research, 2019. **184**: p. 234-242.
564   17.   Patro, R., et al., *Salmon provides fast and bias-aware quantification of transcript*
565   *expression.* Nature methods, 2017. **14**(4): p. 417-419.
566   18.   Soneson, C., M.I. Love, and M.D. Robinson, *Differential analyses for RNA-seq:*
567   *transcript-level estimates improve gene-level inferences.* F1000Research, 2015. **4**.
568   19.   Love, M.I., W. Huber, and S. Anders, *Moderated estimation of fold change and*
569   *dispersion for RNA-seq data with DESeq2.* Genome biology, 2014. **15**(12): p. 1-21.
570   20.   Harrow, J., et al., *GENCODE: the reference human genome annotation for The*
571   *ENCODE Project.* Genome research, 2012. **22**(9): p. 1760-1774.
572   21.   Yates, B., et al., *Genenames. org: the HGNC and VGNC resources in 2017.* Nucleic
573   acids research, 2016: p. gkw1033.
574   22.   Ignatiadis, N., et al., *Data-driven hypothesis weighting increases detection power in*
575   *genome-scale multiple testing.* Nature methods, 2016. **13**(7): p. 577-580.
576   23.   Yu, G., et al., *clusterProfiler: an R package for comparing biological themes among gene*
577   *clusters.* Omics: a journal of integrative biology, 2012. **16**(5): p. 284-287.
578   24.   Robinson, M.D., D.J. McCarthy, and G.K. Smyth, *edgeR: a Bioconductor package for*
579   *differential expression analysis of digital gene expression data.* Bioinformatics, 2010.
580   **26**(1): p. 139-140.
581   25.   Gu, Z., R. Eils, and M. Schlesner, *Complex heatmaps reveal patterns and correlations in*
582   *multidimensional genomic data.* Bioinformatics, 2016. **32**(18): p. 2847-2849.
583   26.   Cowan, C.S., et al., *Cell types of the human retina and its organoids at single-cell*
584   *resolution.* Cell, 2020. **182**(6): p. 1623-1640. e34.
585   27.   Voigt, A.P., et al., *Single-cell transcriptomics of the human retinal pigment epithelium*
586   *and choroid in health and macular degeneration.* Proceedings of the National Academy
587   of Sciences, 2019. **116**(48): p. 24100-24107.
588   28.   Yan, W., et al., *Cell atlas of the human fovea and peripheral retina.* Scientific reports,
589   2020. **10**(1): p. 1-17.
590   29.   Voigt, A.P., et al., *Bulk and single-cell gene expression analyses reveal aging human*
591   *choriocapillaris has pro-inflammatory phenotype.* Microvascular Research, 2020. **131**: p.
592   104031.
593   30.   Swamy, V.S., et al., *Building the mega single cell transcriptome ocular meta-atlas.*
594   bioRxiv, 2021.

595 31. Köster, J. and S. Rahmann, *Snakemake—a scalable bioinformatics workflow engine.*
596   Bioinformatics, 2012. **28**(19): p. 2520-2522.
597 32. Boulton, M. and P. Dayhaw-Barker, *The role of the retinal pigment epithelium:*
598   *topographical variation and ageing changes.* Eye, 2001. **15**(3): p. 384-389.
599 33. Milam, A.H., et al., *Dominant late-onset retinal degeneration with regional variation of*
600   *sub-retinal pigment epithelium deposits, retinal function, and photoreceptor*
601   *degeneration.* Ophthalmology, 2000. **107**(12): p. 2256-2266.
602 34. Hamel, J.-F., *Les ruines du progrès chez Walter Benjamin: anticipation futuriste, fausse*
603   *reconnaissance et politique du présent.* Protée, 2007. **35**(2): p. 7-14.
604 35. Mustafi, D., et al., *Transcriptome analysis reveals rod/cone photoreceptor specific*
605   *signatures across mammalian retinas.* Human molecular genetics, 2016. **25**(20): p. 4376-
606   4388.
607 36. Swamy, V. and D. McGaughey, *Eye in a disk: eyeIntegration human pan-eye and body*
608   *transcriptome database version 1.0.* Investigative ophthalmology & visual science, 2019.
609   **60**(8): p. 3236-3246.
610 37. Efremova, M., et al., *CellPhoneDB: inferring cell–cell communication from combined*
611   *expression of multi-subunit ligand–receptor complexes.* Nature protocols, 2020. **15**(4): p.
612   1484-1506.
613 38. R Sparrrow, J., D. Hicks, and C. P Hamel, *The retinal pigment epithelium in health and*
614   *disease.* Current molecular medicine, 2010. **10**(9): p. 802-823.
615 39. Zou, H., et al., *Polarity and epithelial-mesenchymal transition of retinal pigment*
616   *epithelial cells in proliferative vitreoretinopathy.* PeerJ, 2020. **8**: p. e10136.
617 40. Paterson, E.N., et al., *Association of reduced inner retinal thicknesses with chronic*
618   *kidney disease.* BMC nephrology, 2020. **21**(1): p. 1-12.
619 41. Balmforth, C., et al., *Chorioretinal thinning in chronic kidney disease links to*
620   *inflammation and endothelial dysfunction.* JCI insight, 2016. **1**(20).
621 42. Dewing, J.M., et al., *The Diverse Roles of TIMP-3: Insights into degenerative diseases of*
622   *the senescent retina and brain.* Cells, 2020. **9**(1): p. 39.
623 43. Simeonov, D.R., et al., *DNA variations in oculocutaneous albinism: an updated mutation*
624   *list and current outstanding issues in molecular diagnostics.* Human mutation, 2013.
625   **34**(6): p. 827-835.
626 44. Zou, Z., et al., *Targeted Vezf1-null mutation impairs vascular structure formation during*
627   *embryonic stem cell differentiation.* Arteriosclerosis, thrombosis, and vascular biology,
628   2010. **30**(7): p. 1378-1388.
629 45. Tang, K., et al., *COUP-TFs regulate eye development by controlling factors essential for*
630   *optic vesicle morphogenesis.* Development, 2010. **137**(5): p. 725-734.
631 46. Budi, E.H., L.B. Patterson, and D.M. Parichy, *Embryonic requirements for ErbB*
632   *signaling in neural crest development and adult pigment pattern formation.* 2008.
633 47. Martemyanov, K.A., *G protein signaling in the retina and beyond: the Cogan lecture.*
634   Investigative ophthalmology & visual science, 2014. **55**(12): p. 8201-8207.
635 48. Lee, M., et al., *Hippo☐yap signaling in ocular development and disease.* Developmental
636   Dynamics, 2018. **247**(6): p. 794-806.
637 49. Reyes, A.P., et al., *Identification of cell surface markers and establishment of monolayer*
638   *differentiation to retinal pigment epithelial cells.* Nature communications, 2020. **11**(1): p.
639   1-15.

640   50.   Radeke, M.J., et al., *Disease susceptibility of the human macula: differential gene*
641   *transcription in the retinal pigmented epithelium/choroid.* Experimental eye research,
642   2007. **85**(3): p. 366-380.
643   51.   van Soest, S., et al., *Comparison of human RPE gene expression in macula and periphery*
644   *highlights potential topographic differences in Bruch's membrane.* Mol Vis, 2007. **13**: p.
645   1608-1617.
646   52.   Zhu, S., et al., *Molecular structure, gene expression and functional role of WFDC1 in*
647   *angiogenesis and cancer.* Cell Biochemistry and Function, 2021.
648